HIAPER Cloud Radar (HCR) data, Version 1.2

Changes from Version 1.1

Changes were made to the ECHO_TYPE fields and the MELTING_LAYER field. The ICING_LEVEL field is no longer provided. See “Data processing and quality control” section below for details. The backlobe echo identification algorithm and the radial velocity bias correction method for zenith pointing operations have been further improved.

Overview

This dataset contains HIAPER Cloud Radar (HCR) data collected aboard the NSF/NCAR GV HIAPER (Gulfstream-V High-performance Instrumented Airborne Platform for Environmental Research, HIAPER) (N677F) aircraft during SPICULE (Secondary Production of Ice in Cumulus Experiment). The data were collected during 10 research flights which took place between May 29 and June 25, 2021, over the US Great Plains. For more information on SPICULE, see https://www.eol.ucar.edu/field_projects/spicule.

Flight	Start date	Start time UTC	End date	End time UTC
RF01	2021 05 29	15:15	2021 05 29	19:56
RF02	2021 06 01	16:45	2021 06 01	21:18
RF03	2021 06 02	20:40	2021 06 03	01:23
RF04	2021 06 05	13:46	2021 06 05	21:59
RF05	2021 06 09	19:50	2021 06 09	23:34
RF06	2021 06 11	17:45	2021 06 12	00:03
RF07	2021 06 17	18:20	2021 06 18	00:44
RF08	2021 06 20	18:50	2021 06 21	04:00
RF09	2021 06 24	19:55	2021 06 24	23:46
RF10	2021 06 25	18:45	2021 06 25	22:49

Instrument description

HCR (NCAR/EOL HCR Team, 2014) is an airborne, polarimetric, millimeter-wavelength (W-band) radar that serves the atmospheric science community by providing cloud remote sensing capabilities to the NSF/NCAR G-V (HIAPER) aircraft. HCR detects drizzle, and ice and liquid clouds, and collects Doppler radial velocity measurements, which at vertical incident include the vertical wind speed and particle fall speed.

In a pod-based design, a single lens antenna is used for both transmit and receive. The transceiver uses a two-stage up and down conversion superheterodyne design. The transmit

waveform, from a waveform generator, passes through the two-stage up-conversion to the transmit frequency of 94.40 GHz. It is then amplified by an extended interaction klystron amplifier (EIKA) to 1.6 kW peak power. System performance on transmit and receive paths are closely monitored using a coupler and a noise source. Raw in-phase and quadrature information are archived in HCR. For more information, see Vivekanandan et al. (2015) and www.eol.ucar.edu/instruments/hiaper-cloud-radar-hcr

HIAPER Cloud Radar Specifications	
Parameter	**Specification**
Antenna	0.30 m, lens
Antenna gain	46.21 dB
Antenna 3 dB beam width	0.73°
Transmit Polarization	Linear (V)
Transmit frequency	94.40 GHz
Transmitter	Klystron
Peak transmit power	1.6 kW
Pulse width	0.2 – 1.0 μs
PRF	up to 10 kHz
System noise power	-101 dBm
Receiver noise figure	8.9 dB
Receiver Bandwidth	20 MHz
Receiver Dynamic Range	76 dB
First IF	156.25 MHz
Second IF	1406.25 MHz
Range resolution	20 - 180 m
Unambiguous range	15 km
Typical reflectivity uncertainty	0.4 dB
Sensitivity	-35.0 dBZ at 1 km and 256 ns pulse
Unambiguous velocity	±7.75 m/s
Typical radial velocity uncertainty	0.2 m/s at W=2 m/s
Dwell time	100 ms

Data description

The 10 Hz moments data described here are available at http://data.eol.ucar.edu/dataset/605.011. in CfRadial format. For more information on CfRadial see www.ral.ucar.edu/projects/titan/docs/radial_formats/CfRadialDoc.pdf.

The primary data products for scientific use are listed in the table below.

Variable	Dimensions	Unit	Long Name
time	time	seconds	Time in seconds since volume start
range	time	meters	Range from instrument to center of gate
latitude	time	deg	Latitude
longitude	time	deg	Longitude
altitude	time	meters	Altitude of radar
DBZ	time, range	dBZ	Reflectivity
DBZ_MASKED	time, range	dBZ	Reflectivity of cloud echo only (DBZ(FLAG>1)=NAN, see FLAG below)
VEL_MASKED	time, range	m/s	Motion and bias corrected and de-aliased Doppler velocity
WIDTH	time, range	m/s	Spectral width
SNR	time, range	dB	Signal to noise ratio
DBMVC	time, range	dBm	Log power co-polar v transmit, v receive
DBMHX	time, range	dBm	Log power cross-polar v transmit, h receive
NCP	time, range		Normalized coherent power
LDR	time, range	dB	Linear depolarization ratio (V/H)
PRESS	time, range	hPa	Air pressure from ERA5
TEMP	time, range	C	Air temperature from ERA5
RH	time, range	%	Relative humidity from ERA5
SST	time	C	Sea surface temperature from ERA5
U	time, range	m/s	U wind component from ERA5
V	time, range	m/s	V wind component from ERA5
TOPO	time	m	Terrain elevation above mean sea level from GTOPO30
FLAG	time, range		See Romatschke et al. (2021) Flag field to classify reflectivity (to mask unwanted data): 1 Cloud 2 Speckle (contiguous 2D echo areas of < 100 pixels) 3 Extinct (signal completely attenuated) 4 Backlobe echo (reflection from the land/sea surface when zenith pointing and flying low)

			5 Out of range (second trip echo from land/sea surface when flying too high) 6 Transmitter pulse (echo from within the radar itself) 7 Water surface echo 8 Land surface echo 9 Below the surface 10 Noise source calibration 11 Antenna in transition (e.g. from nadir to zenith or vice versa) 12 Missing (not transmitting)
ANTFLAG	time		Flag field to indicate the status of the antenna: 1 Down (nadir pointing) 2 Up (zenith pointing) 3 Pointing (pointing to an angle different from nadir or zenith) 4 Scanning (e.g. sea surface calibration) 5 Transition (e.g. from nadir to zenith) 6 Failure
MELTING_LAYER	time, range		See Romatschke (2021) but note changes described in the next section 9 warm 11 melting warm 19 melting cold 21 cold
ECHO_TYPE_2D	time, range		See Romatschke and Dixon (2022) 14 stratiform low 16 stratiform mid 18 stratiform high 25 mixed 30 convective 32 convective elevated 34 convective shallow 36 convective mid 38 convective deep
ECHO_TYPE_1D	time		As ECHO_TYPE_2D
PID	time, range		See Romatschke and Vivekanandan (2022) 1 rain 2 supercooled rain 3 drizzle 4 supercooled drizzle 5 cloud liquid 6 supercooled cloud liquid 7 melting 8 large frozen 9 small frozen

			10 precipitation 11 cloud

Data processing and quality control

A detailed description of the data processing and quality control procedures can be found in Romatschke et al. (2021). The basic principle of the melting layer detection algorithm is described in Romatschke (2021) but significant changes have been made since then (see below). The algorithm that separates radar echo into convective and stratiform types and calculates convectivity is described in Romatschke and Dixon (2022) and the particle identification algorithm is described in Romatschke and Vivekanandan (2022). Changes made since the publication of these papers are described in the following.

Radial velocity

A velocity de-aliasing scheme has been developed and was applied in the VEL_UNFOLDED field. Data from times when HCR was in ANTSTAT modes other than “zenith” or “nadir” were then masked out and the resulting field is available as VEL_MASKED. We recommend using VEL_MASKED as the standard radial velocity field for most purposes.

Based on a method developed by Litai Kang, Robert Wood, and Roger Marchand from the University of Washington, we developed a bias correction algorithm for radial velocity for times when HCR is operating in zenith pointing mode. Similar to the assumption that the land/ocean surface is stationary, which is used to correct radial velocity in nadir pointing operations (Ellis et al., 2019; Romatschke et al., 2021), we assume that cloud top velocities of zenith pointing times are similar to those of the surrounding nadir pointing times. First, cloud top velocities are calculated from the corrected nadir pointing data. These nadir cloud top velocities are then compared to those from the zenith pointing times and a difference between the nadir and zenith pointing cloud top velocities is used for bias correction of the zenith pointing velocity data.

ERA5 reanalysis

The U and V ERA5 reanalysis wind components are now provided on the whole 2D time-range grid instead of just at the surface.

Melting layer detection

A new melting layer detection algorithm has been developed which identifies the whole vertical extent of the melting layer based on a fuzzy logic methodology. The output has been simplified from what is described in Romatschke (2021). The MELTING_LAYER field now has the following flag values: 9 - warm (below the melting layer), 11 - melting warm (in the melting layer but below the altitude of maximum melting), 19 - melting cold (in the melting layer but above the altitude of maximum melting), 21 - cold (above the melting layer). Values of MELTING_LAYER

are set to “missing” outside of regions with cloud echo (i.e., in regions where FLAG does not equal 1). The 1D ICING_LEVEL field is no longer provided because it can easily be derived from the new MELTING_LAYER field.

Stratiform/convective echo type

In the advanced echo classification, where the troposphere is separated into the low, mid, and high region, we do no longer allow the separation boundary between the low and the mid region to fall below 2 km above the ground, and the separation boundary between the mid and the high region to fall below 4 km above ground. This way, we always retain all three regions and the associated cloud classifications, even when the melting layer intersects the ground. See Romatschke (2023) for details.

PID

In the Particle IDentification (PID) field a temperature threshold of -40 °C was set. Liquid particles are no longer allowed at temperatures below this threshold and were set to “precipitation” or “cloud”.

Known problems

Radial velocity

The surface based velocity correction worked well the majority of the time, however there are some regions in which problems were noted. These problems manifest themselves as columns of biased radial velocity at each range bin over several rays. We think these velocity pillars are caused by the filtering process over-smoothing surface velocity variations due to variable pointing error (Ellis et al. 2019). The zenith pointing correction is much less detailed than the nadir pointing correction and only corrects for major biases.

Another problem that cannot be corrected is, that the radar, while it rotates 360˚ around the along-plane axis, has only limited range of motion along the cross-plane axis. This means, that when the aircraft has significant pitch, e.g. during steep climbs, the tilt angle correction of the radar is not sufficient, reports erroneous angles, and the first step of the velocity correction fails. Times when this was the case are masked out in VEL_MASKED and we therefore strongly recommend to only use the VEL_MASKED velocity field.

Backlobe echo in zenith pointing operations

When the HCR is pointing at zenith and the GV is near the surface, there is often an echo that results from the backlobe of the radar reflecting off of the surface. This backlobe contamination is typically characterized by a band of low reflectivity, highly variable radial velocity, and high spectrum width. The backlobe appears in the zenith data at a range equal to the altitude of the

radar. So as the GV ascends or descends the backlobe contamination will recede and approach in range, respectively. An attempt was made to identify the backlobe echo and flag it in the FLAG field but the identification process does not always completely remove all backlobe echo.

Periods during which the HCR transmitter was disabled

In the HCR data, there are some short periods during which the transmitter was disabled for safety reasons. These show up as gaps in the power fields.

H-channel problem

Starting in RF5 HCR experienced problems in the H-channel (the cross-polar channel) which manifested as an increase in the noise floor and stripes in the H fields. The problem occurred intermittently throughout the rest of the project. The main variables affected are DBMHX and LDR. We developed a method to greatly reduce the effects in LDR that is applied to create the LDR_MASKED field (which shows only cloud data, as do the other MASKED fields) but caution is still advisable. Fortunately the problem occurred mostly during clear air periods and only very few cloudy times were affected. The most serious example is shown below.

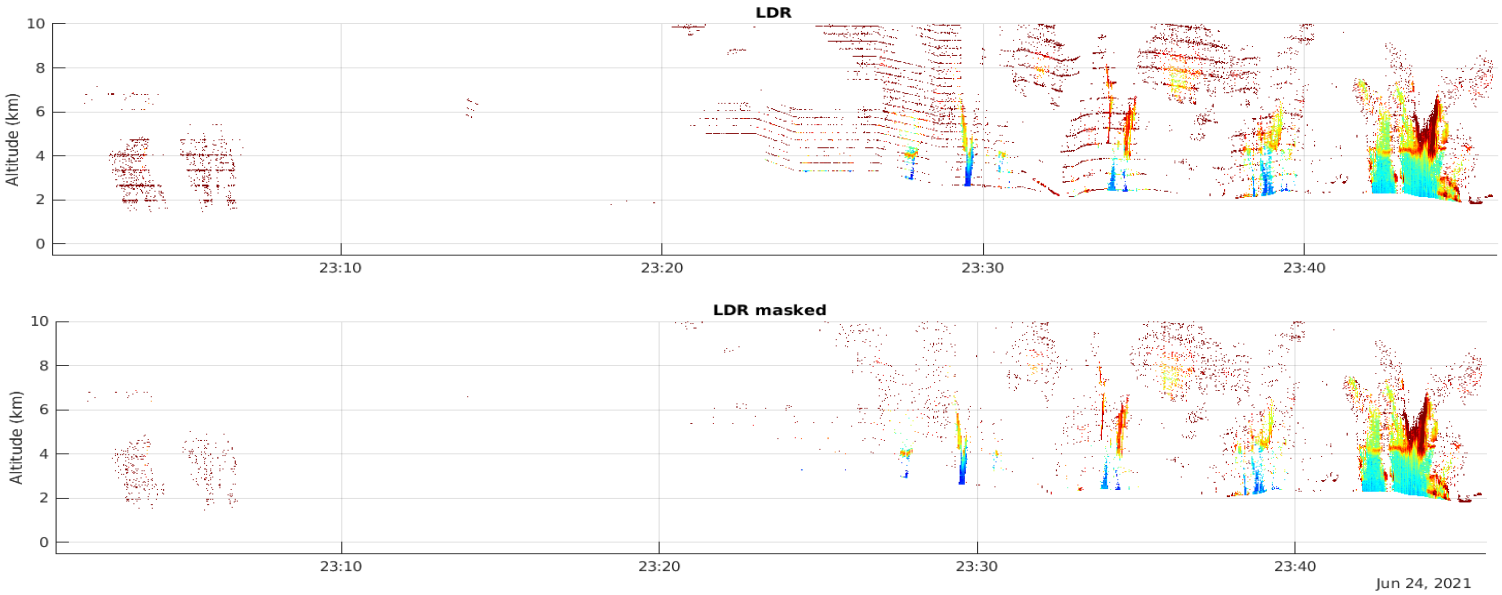

Multiple scattering

In areas of heavy convection HCR data is affected by multiple scattering. Affected areas show increased LDR as seen in the example below. Reflectivity in these areas is likely not accurate and should be used with caution. PID is likely also not correct. We are currently investigating the multiple scattering problem and hope to have more information in the future.

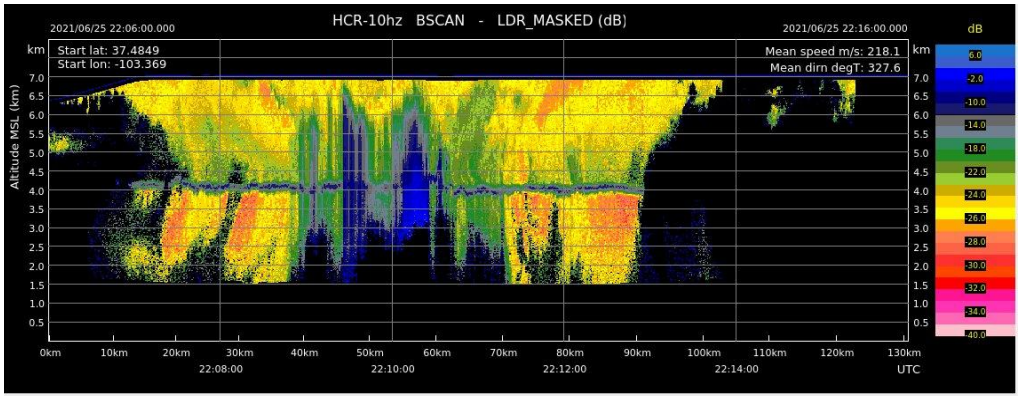

Melting layer detection

While overall, the new melting layer detection algorithm is more robust than the previous one, there are some cases of false identifications of the melting layer.

References

Ellis, S.M., P. Tsai, C. Burghart, U. Romatschke, M. Dixon, J. Vivekanandan, J. Emmett, and E. Loew, 2019: Use of the Earth's Surface as a Reference to Correct Airborne Nadir-Looking Radar Radial Velocity Measurements for Platform Motion. J. Atmos. Oceanic Technol., 36, 1343–1360, https://doi.org/10.1175/JTECH-D-19-0019.1

NCAR/EOL HCR Team. (2014). HIAPER Cloud Radar (HCR). UCAR/NCAR - Earth Observing Laboratory. https://doi.org/10.5065/D6BP00TP

Romatschke, U., M. Dixon, P. Tsai, E. Loew, J. Vivekanandan, J. Emmett, R. Rilling, 2021: The NCAR Airborne 94-GHz Cloud Radar: Calibration and Data Processing. Data, 6, 66. https://doi.org/10.3390/data6060066

Romatschke U., 2021: Melting Layer Detection and Observation with the NCAR Airborne W-Band Radar. Remote Sensing. 13(9):1660. https://doi.org/10.3390/rs13091660

Romatschke, U., Vivekanandan, J., 2022: Cloud and Precipitation Particle Identification Using Cloud Radar and Lidar Measurements: Retrieval Technique and Validation. Earth and Space Science, 9, e2022EA002299. https://doi.org/10.1029/2022EA002299

Romatschke, U., and Dixon, M. J, 2022.: Vertically Resolved Convective/Stratiform Echo Type Identification and Convectivity Retrieval for Vertically Pointing Radars. Journal of Atmospheric and Oceanic Technology, 39, 11, 1705-1716. https://doi.org/10.1175/JTECH-D-22-0019.1

Romatschke, U., 2023: Cloud properties derived from airborne cloud radar observations collected in three climatic regions. Journal of Geophysical Research: Atmospheres, 128, e2023JD039829. https://doi.org/10.1029/2023JD039829

Vivekanandan, J., Ellis, S., Tsai, P., Loew, E., Lee, W.-C., Emmett, J., Dixon, M., Burghart, C., and Rauenbuehler, S., 2015: A wing pod-based millimeter wavelength airborne cloud radar, Geosci. Instrum. Method. Data Syst., 4, 161-176, https://doi.org/10.5194/gi-4-161-2015

Citation

NCAR/EOL Remote Sensing Facility. 2022. SPICULE: NCAR HCR radar moments data. Version 1.1. UCAR/NCAR - Earth Observing Laboratory. https://doi.org/10.26023/PGGK-MC4T-K70F. Accessed <YYYY-MM-DD>.

Contact

EOL Data Support: eol-datahelp@ucar.edu

UCAR/NCAR - Earth Observing Laboratory
Remote Sensing Facility
HIAPER Cloud Radar
http://doi.org/10.5065/D6BP00TP